Disaggregated PROBA-V data allows monitoring individual crop phenology at a higher observation frequency than Sentinel-2

Henry Rivas, Nicolas Delbart, Catherine Ottlé, Fabienne Maignan, Emmanuelle Vaudour

International Journal of Applied Earth Observations and Geoinformation 104 (2021) 102569

Contents lists available at ScienceDirect

International Journal of Applied Earth Observations and Geoinformation

journal homepage: www.elsevier.com/locate/jag

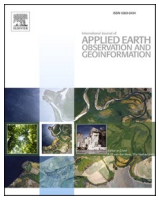

Disaggregated PROBA-V data allows monitoring individual crop phenology at a higher observation frequency than Sentinel-2

Henry Rivas [a,*], Nicolas Delbart [a], Catherine Ottlé [b], Fabienne Maignan [b], Emmanuelle Vaudour [c]

[a] Université de Paris, CNRS, Laboratoire Interdisciplinaire des Energies de Demain, 75013 Paris, France
[b] Université Paris-Saclay, CNRS, CEA, UVSQ, Laboratoire des Sciences du Climat et de l'Environnement, 91191 Gif-sur-Yvette, France
[c] Université Paris-Saclay, INRAE, AgroParisTech, ECOlogie fonctionnelle et écotoxicologie des agroécoSYStèmes, 78850 Thiverval-Grignon, France

ARTICLE INFO

Keywords:
Spatial disaggregation
Linear unmixing
Phenometrics
Crop phenology mapping

ABSTRACT

Satellite-based monitoring of crop phenology is commonly built on the analysis of Vegetation Index (VI) time series by extracting phenological metrics. The relatively fine detection of the various timings in crops growth during their development cycle depends on the density and regularity of valid observations. Medium spatial resolution (MSR) daily observations provide consistent cloud-free n-day composite time series, suitable for phenological applications, but do not offer an adequate spatial resolution. MSR pixels are generally mixed pixels or "mixels", composed of several land cover classes, which complicate crop-specific monitoring from space. To address the MSR mixel problem, we implemented a spatial disaggregation (SD) approach that estimates a crop-specific VI based on the crop fraction in a mixel provided by a land use map. First, SD was applied on synthetic MSR data (i.e. Sentinel-2 data aggregated at 300 m) in order to test the method in an ideal case. After validation, the method was applied to PROBA-V data, using 300 m and 10-day composites over a large area around Paris, for four main crops (i.e. winter cereals, spring barley, oilseed rape and maize) in 2016–2017. The evaluation of SD was done by comparing disaggregated data with reference data (i.e. Sentinel-2 10 m). Indeed, two main results were observed, i) SD was able to reconstruct the crop-specific VI time series of all crops and ii) PROBA-V data increased the number of crop-specific VI valid observations at certain stages of the crop's growth period compared to Sentinel-2 data, this with a consistent and regular revisit throughout the growth cycle. In conclusion, SD can be used to improve the exploitation of MSR data in seasonal crop monitoring, especially during the transition periods when the VI of crops are likely to change quickly. This paves the way for monitoring crop phenology over fragmented landscapes, from sensors such as MODIS or SPOT-VEGETATION, even for years before Sentinel-2 launch.

1. Introduction

Crop monitoring has been at the core of the motivations for developing Earth Observation satellites like Landsat since the 1970's. Remote sensing data have frequently been used for many applications in the agricultural sector, ranging from near-real time crop monitoring to yield forecasting for examples, as detailed by Atzberger (2013) and Weiss et al. (2020). Reasons for monitoring crops by remote sensing are numerous. First, remote sensing brings essential knowledge for food production evaluation such as main crop types, cultivated areas or yields (e.g. Donohue et al., 2018; Lobell, 2013; Lobell et al., 2015; Wu et al., 2014). Second, real time monitoring can support crop management and agricultural practices (e.g. Dodin et al., 2021; Mulla, 2013). Third, it provides indicators for agro-ecosystems assessment on hydrology (e.g. Baghdadi et al., 2008; Leenhardt et al., 2012), biodiversity (e.g. Petrou et al., 2015), soil organic carbon (e.g. Vaudour et al., 2021), pollution by pesticides (e.g. Ward et al., 2000), etc.

Since crop development is highly dynamic during its vegetation cycle, a large part of remote sensing agricultural applications rely on the ability to frequently acquire images. This is necessary to monitor radiometric temporal changes linked to crop growth, which allows main crop types identification (Foerster et al., 2012; Heupel et al., 2018; Siachalou et al., 2015; Vaudour et al., 2015; Waldner et al., 2016) or agricultural production assessment (Becker-Reshef et al., 2010; Wu et al., 2014). Monitoring growth development stages, mostly known as crop phenology, is one of most important agricultural applications of

* Corresponding author.
E-mail address: henry-david.rivas-ullon@etu.u-paris.fr (H. Rivas).

https://doi.org/10.1016/j.jag.2021.102569
Received 3 June 2021; Received in revised form 27 September 2021; Accepted 1 October 2021

remote sensing (Atzberger, 2013).

The monitoring of vegetation phenology largely relies on medium spatial resolution (MSR), i.e. hectometric to kilometric, satellite images (Becker-Reshef et al., 2010; Delbart et al., 2015, 2006, 2005; Sakamoto et al., 2006, 2005). This is because MSR sensors acquire data across a large swath allowing an almost complete coverage every day, at least outside the tropics. Indeed, transitional vegetation phases can be observed with a high revisit level depending on the satellite temporal resolution and cloud cover status. Daily measurements also increase the probability of cloud-free composite images, which reinforces the ability to monitor phenology with such sensors. However, MSR satellite series are best suited to large scale applications (wide regions, and/or national to semi-continental scales) for relatively homogeneous landscapes characterized by large areas, such as open fields (Kastens et al., 2017). For agricultural landscapes characterized by smaller fields, MSR pixels are generally mixed pixels or "mixels". This makes crop-specific monitoring more complex, as in the fragmented landscapes of north-western France where field size is around 6.5 ha in average.

In this context, phenological indicators detection in such areas requires observations with high spatial resolution (HSR), which limits the possible contribution of adjacent fields in a given pixel. In addition, the identification of phenological transitional stages needs a high revisit frequency, and images should be taken every 10 days at least, which makes recent satellite series such as Sentinel-2 well suited (Defourny et al., 2019; Khaliq et al., 2018; Solano-Correa et al., 2018).

Yet, Sentinel-2 data have several limitations, particularly for retrospective phenology studies. Since 2015 only, data are available with a 10-day temporal resolution, then with a 5-day one from 2017 onwards. In temperate areas, temporal frequency of usable observations might be lower because of cloud cover, notably in autumn when winter crops start growing.

To address the MSR mixel problem, many solutions have been proposed based on spatial downscaling models aiming at extracting fine resolution information from coarse resolution products, with the help of fine resolution auxiliary data. In the case of vegetation phenology, land cover maps at high resolution are generally used. Spatial downscaling, also called disaggregation, fusion or unmixing methods, can rely on very different techniques from purely statistical to physically-based ones. The overall purpose is to solve the linear or nonlinear spectral unmixing problem assuming that the mixel variable is the combination of the endmember signals weighted by their respective fractions. Such approaches have been developed to unmix spectral reflectances of various sensors. For example, Gao et al. (2006) proposed the STARFM model to predict daily reflectances at Landsat spatial resolution from a set of Landsat and MODIS data. The method has been extended and tested with success to map crop phenology and land cover at 30 m resolution using vegetation index (NDVI) time series (Gao et al., 2017). Inspired by STARFM, Gevaert and García-Haro (2015) and Zhao et al. (2018) proposed the STRUM and RASTFM methods respectively to unmix spectral reflectances. Compared to STARFM, these methods showed better performances when i) the availability of high spatial resolution imagery is limited and ii) complex spatio-temporal changes, such as urban expansion, are present. The same approaches have been applied to the downscaling of FAPAR (fraction of absorbed photosynthetically active radiation) satellite products. For example, Li et al. (2017) fused Landsat and PROBA-V (300 m) to estimate FAPAR at 30 m via a second-degree empirical polynomial function and were able to increase the spatio-temporal resolution and fill cloud gaps in the Landsat-like FAPAR time series. The unmixing problem has also been addressed through deterministic approaches such as the one proposed by Lobell and Asner (2004), who assessed the temporal reflectances of the endmembers provided by pure MODIS pixels to map cropland fractions in their mixels. The method demonstrated good performances at regional scale but could display high uncertainties at a finer scale. On their side, Haertel and Shimabukuro (2005) proposed a "double step inversion". First, endmembers' fractions were estimated in Landsat mixels from their reflectances provided by pure pixels. Then, the fractions were aggregated at MODIS resolution and their endmembers reflectances were estimated. They obtained satisfactory results on the endmembers reflectances in all the spectral bands used. Busetto et al. (2008) estimated the endmembers signals to generate NDVI time series at the MODIS sub-pixel level using a weighted system of equations based mainly on the spectral dissimilarity of the mixels with the target pixel provided by Landsat. It showed greater accuracy as the endmember fraction increased in the mixel. On the other hand, statistical approaches have also been explored. For example, Faivre and Fischer (1997) assumed that crop reflectances within a land cover class were Gaussian and could be estimated by a Bayesian inversion approach. The method was applied successfully to predict crop reflectances at 20 m spatial resolution from degraded SPOT data at 400 m.

Here, a SD method was implemented for disaggregating the NDVI (Normalized Difference Vegetation Index) of agricultural mixels in order to reconstruct crop-specific NDVI temporal profiles from MSR time series, using the crop fraction provided by a land use map as auxiliary data. Similar to Asner et al. (1997), Atzberger et al. (2014), etc. studies, this approach was based on a classical linear mixing model.

2. Study area, materials and methods

2.1. Study area

The study area is a cropland located in the northern half of the Ile-de-France administrative region, around Paris (48°65′ − 49°25′ N; 1°65′ − 3°10′ E) and comprises a total area of 7 039 km2. The boundaries of the study area were defined by the Sentinel-2 T31UDQ tile (Fig. 1). Crop rotations mostly comprise winter oilseed rape, winter wheat, spring barley and sometimes maize. Crop production conventionally starts from deep ploughing in November-December, then chisel in March, followed by seedbed preparation for spring cereals. Winter crops are typically sown in October-November and spring crops in March-April.

2.2. Materials: Satellite imagery and land use map

All the available scenes from Sentinel-2 and PROBA-V sensors between September 2016 and October 2017 were used. Sentinel-2 (A and B) images were acquired at 10 m spatial resolution with a five days revisit interval. The level 2A images that provide surface reflectances with atmospheric corrections were downloaded from the Muscate platform of the French land data center (CNES-THEIA LAND, n.d). NDVI time series were computed and included 54 scenes. Synthetic MSR data were built by the averaging resampling method to aggregate Sentinel-2 NDVI images at a 300 m spatial resolution.

PROBA-V images were acquired at 300 m spatial resolution with a daily revisit. In this study, the S10 10-day composite NDVI product, based on the Maximum Value Composite method as proposed by Holben (1986), was used. The products were obtained from the Vito Remote Sensing data center (VITO, 2018). NDVI time series included 42 scenes. All images from the two sensors were masked from clouds and shadows.

The land use map was obtained from the Land Parcel Identification System (LPIS). Since 2015 in France, LPIS has provided an annual map of crop types reported at the field level. The database was downloaded from the Géoservices platform of the *Institut national de l'information géographique et forestière* (IGN, 2021). The four following thematic crop classes were considered: winter cereals (grouping winter wheat and winter barley), winter oilseed rape, maize and spring barley (Table 1). In addition, a fifth class named "others" was created to refer to the remaining land cover types of the agricultural landscape, such as other crop types, rural ways, herbaceous or non-herbaceous inter-parcel boundaries, hedges, small urbanized areas, groves, etc.

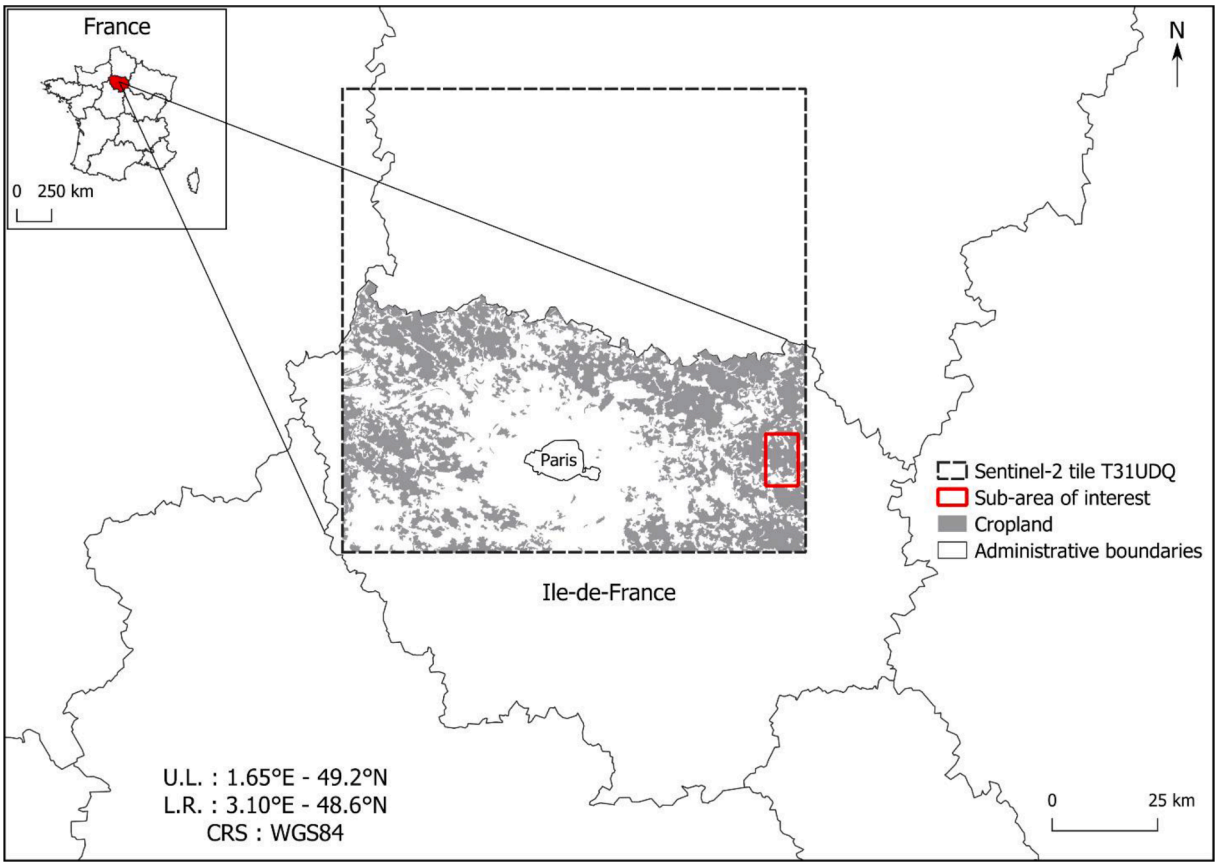

Fig. 1. Location of the study area within the Ile-de-France administrative region. The red box delimitates the sub-area of interest presented in Fig. 4. (For interpretation of the references to colour in this figure legend, the reader is referred to the web version of this article.)

Table 1
Area covered by the four main crops under study.

Main crop	Total area (ha)	Average field area (ha)	% of cultivated land
Winter cereals	106 000	7.3	48.3
Winter oilseed rape	28 926	7.5	13.1
Maize	17 782	5.0	8.1
Spring barley	8 790	5.4	4.0

2.3. Methods

The SD algorithm was applied on synthetic MSR data knowing crop fractions within mixels through the LPIS. Sentinel-2 with 10 m spatial resolution was used to evaluate the results. The SD method was further applied on real MSR PROBA-V data (Fig. 2).

2.3.1. Mathematical principles

The SD method was based on the linear mixing model, which assumes that the signal value of a mixel j is the weighted average of the contribution of each land use i fraction present within that mixel j, and that the signal is stationary within a land use class as detailed by Settle and Drake (1993). This approach was applied to the NDVI, with the contribution of each crop type i to the $NDVI_j$ value weighted by its fractional coverage, which is mathematically expressed as follows:

$$NDVI_j(t) = \sum_{i=1}^{n} fc_{i,j} \times NDVI_i(t) + \varepsilon_j(t) \quad (1)$$

where $NDVI_j(t)$ is the NDVI value of the mixel j at time t, $fc_{i,j}$ is the areal fraction of crop i in mixel j, $NDVI_i(t)$ is the NDVI value of crop i at time t, n is the number of crops within mixel j, and $\varepsilon_j(t)$ is the error in mixel j at time t.

Oleson et al. (1995) proposed to build a system of linear equations, replicating Eq. (1), from all pixels k in a neighborhood. Therefore, the $NDVI_i(t)$ estimate can be given by solving a system of M linear equations using pseudo-inversion (since generally $M > n$) as follows:

$$NDVI_i(t)_{(n\times 1)} = \left[fc^t_{(M\times n)} fc_{(M\times n)}\right]^{-1} fc^t_{(M\times n)} NDVI_j(t)_{(M\times 1)} \quad (2)$$

where $fc_{(M\times n)}$ is the matrix of fractions with M number of rows (corresponding to the number of mixels considered for the estimation) and n number of columns (corresponding to the number of analyzed crop types).

2.3.2. Spatial disaggregation method

Input data comprised a generic MSR satellite image obtained at a given time t $(MSRimage_t)$, and yearly images of fractional cover per thematic crop class (fc_i) matched at the same spatial resolution. For each mixel j of the $MSRimage_t$, both $NDVI_j$ value and areal fraction values of its sub-pixels $\left(fc_{i,j}\right)$ were known. This allowed to build the $M-$system from which the NDVI value of each class i was estimated (Fig. 3).

2.3.2.1. Fractional cover image. The fractional cover image $(fc_{i,j})$ represented the fraction of thematic crop class i within each mixel j of the MSR image. The areal fractions of the classes present within mixels were obtained by intersecting a grid at MSR resolution with the land use map of thematic crop classes. Based on intersected pixels, MSR image target mixels containing one or more classes of interest (Table 1) to be processed were identified. The sum of all classes i fractions within a mixel j must be equal to $1\left(\sum_{i=1}^{n} fc_{i,j} = 1\right)$.

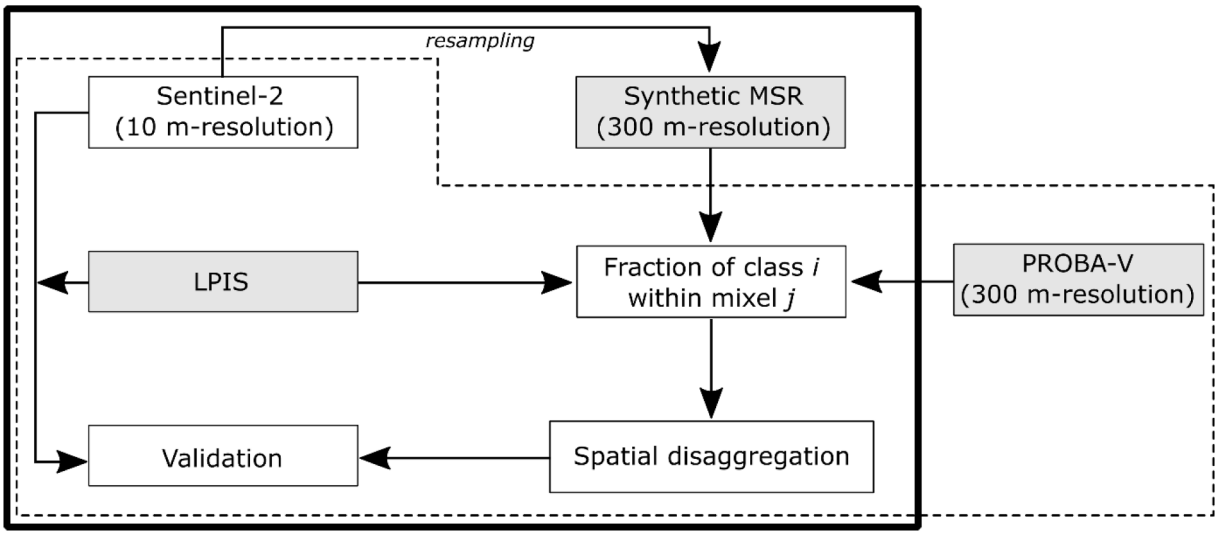

Fig. 2. Methods workflow. The solid box represents the development section of the SD algorithm on synthetic MSR data. The dotted box represents the application section of the SD algorithm on real MSR PROBA-V data. Shaded boxes figure input data. The SD algorithm (bottom right box) is detailed on Fig. 3.

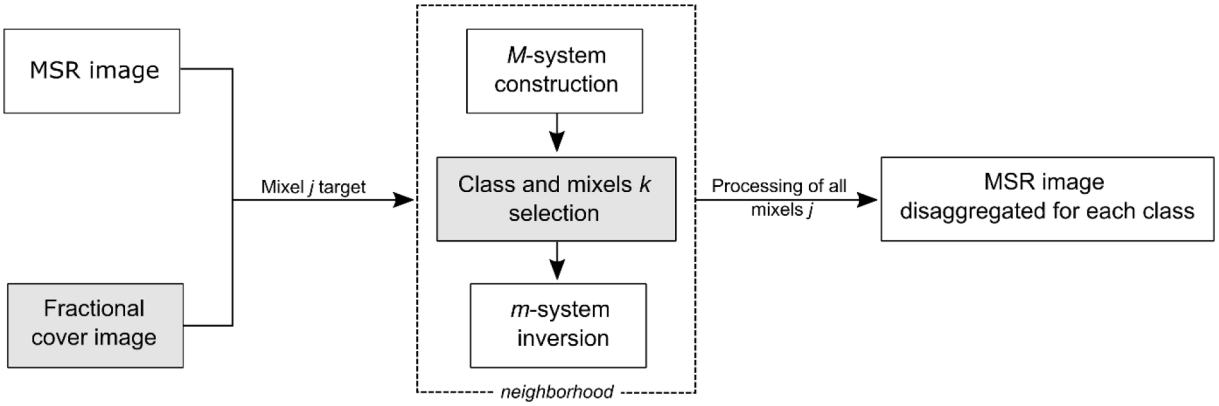

Fig. 3. SD algorithm framework. Shaded and dotted boxes are detailed in the sections below.

2.3.2.2. Class and mixels selection. All neighboring mixels *k* that built a given *M*-system were composed of the same thematic crop classes *i* as the central target mixel *j*. The "matched" composition between target mixel *j* and a mixel *k* was one of all possible combinations of classes *i* present in the target mixel. Indeed, if mixel *j* was composed of three classes (a, b, c), a selected neighbor pixel had the same or a lower number of classes than the mixel *j* (e.g. a, b; a, c; b, c; a, b, c or pure pixel). In addition, mixels *k* that did not meet class *i* minimum fraction criteria (i.e. 0.01) were excluded from *M*-system. Consequently, a new subset of mixels *k* called *m*-system was obtained, which was used to estimate the $NDVI_i$ of a target mixel *j*.

2.3.2.3. SD application at neighborhood level. The crop-specific $NDVI_i$ value of a target mixel *j* was estimated from neighboring mixels *k* in order to preserve the spatial variability of the classes *i* across the study area as proposed by Zhukov et al. (1999). Therefore, the algorithm considered that NDVI value of class *i* at time *t* in mixel *j* may be different from that of mixel *k* belonging or not to the same close neighborhood $(NDVI_{i,j} \neq NDVI_{i,k})$. Differences in NDVI values may stem either from pedoclimatic/environmental variability, or from management practices (e.g. plant material, fertilization, cultural operations, irrigation, amendment practices, etc.). In order to better reflect the considered pixel, the *M*-system was built using a sliding window of size 3 × 3, restricting the disaggregation process to its closest neighborhood.

2.3.3. Evaluation: Comparing disaggregated data with reference data

SD performance was evaluated by comparing NDVI temporal profile with the reference data. Comparison was made for each disaggregated mixel *j* for each crop type *i* on a pixel-by-pixel basis. Reference data were the average NDVI of class *i* in a mixel *j* provided by pure Sentinel-2 pixels with full 10 m spatial resolution. Performance indicators used were correlation coefficients (R, Eq. (3)) and root mean square differences (RMSD, Eq. (4)). Sentinel-2 and PROBA-V comparison was made between closest acquisition dates (i.e. ± 5 days).

$$R = \frac{\sum_{i=1}^{n}(x_i - \bar{x})(y_i - \bar{y})}{\sqrt{\sum_{i=1}^{n}(x_i - \bar{x})^2}\sqrt{\sum_{i=1}^{n}(y_i - \bar{y})^2}} \quad (3)$$

$$RMSD = \sqrt{\frac{1}{n}\sum_{i=1}^{n}(x_i - y_i)^2} \quad (4)$$

where *n* is the number of dates, *x* is the reference NDVI value of crop type *i* of mixel *j*, and *y* is the disaggregated NDVI value of crop type *i* of mixel *j*.

3. Results

Results are presented in three steps: i) description of the disaggregated crop-specific images; ii) analysis of the level of agreement of

the temporal NDVI profile between disaggregated and reference data and iii) average temporal profiles of all disaggregated mixels.

3.1. Disaggregated crop-specific image

SD main results were the disaggregated crop-specific images. Fig. 4 shows a sub-region of such images for winter cereals and maize at two dates (26th May and 29th August 2017). Overall, output maps suggested the ability of the SD method to reconstruct spatio-temporal growth dynamics for a given crop. The NDVI temporal behaviour reflected seasonal weather variations reproducing the large differences that can be observed from spring to summer periods (Fig. 4). May image shows the peak of vegetative activity in the winter cereals cycle while the August image corresponds to post-harvest. Referring to maize, it was sown in April-May and harvested in October. The maize fields appear bare on the 26th May image while the 29th August image shows a peak of vegetative activity.

3.2. Disaggregated crop-specific time series vs reference data

On a mixel *j* level (Fig. 5), SD allowed retrieving the different seasonality of winter cereals and maize. SD reproduced the large differences in NDVI observed by Sentinel-2 during the autumn and spring periods. It shall be specified that, because its composition was not homogeneous with that of the other pixels in the 3x3 pixels neighborhood, the mixel *k* at the bottom right containing winter oilseed rape was not considered in the estimation. Disaggregated NDVI profiles of the central mixel *j* in Fig. 5 were obtained from the *m*-system relying on the 7 neighboring pixels and the central mixel *j* itself.

Overall, considering both RMSD and correlation maps of performance, a high level of agreement was obtained between the disaggregated time series and reference data for all crops and for the entire study area (Fig. 6).

3.3. Average temporal NDVI profiles of all disaggregated mixels

The average NDVI profile, over the entire study area, of all disaggregated mixels for a given crop made it possible to summarize results with respect to the temporal behaviour. Fig. 7 demonstrates the capability of the SD algorithm to reproduce the temporal variations captured by Sentinel-2 with 10 m spatial resolution. These temporal variations, depending on the crop types, designate the different phenological stages that can be retrieved by remote sensing (i.e. SOS, POS and EOS).

The start of the growing season of winter cereals was detectable from a few weeks after the emergence of the plants (Fig. 7a). NDVI values began to rise in December; then, the NDVI peak occurred between May and June during stages with maximum leaf biomass and chlorophyll activity. The end of the cycle was marked by the start of the senescence in mid-June. For spring crops, a consistent change in NDVI was visible in April-May for spring barley and May-June for maize (Fig. 7d and c). Spring barley was harvested at the same time as winter crops in late July, while maize was harvested in late October. The winter oilseed rape began its cycle in September and was harvested at the end of July. Its flowering took place between April and May. Such a phenological event could be linked to the observed decrease of about $\approx$ 20% in NDVI amplitude during this period (Fig. 7b).

3.4. Application of SD algorithm on PROBA-V data

Similarly to the outputs from the synthetic MSR data, SD applied on PROBA-V with a 300 m spatial resolution was able to correctly reproduce the temporal variations of NDVI for all crops. Temporal behaviours of disaggregated mixels strongly matched the reference data (Fig. 8). One striking improvement from SD over the Sentinel-2 data was the regularity of the observations and their densification over periods during which no cloud-free Sentinel-2 data were available. For example, there was no cloudless Sentinel-2 data available in October and November 2016, while SD allowed monitoring the initial growth of winter oilseed rape during this specific period (Fig. 8). Figs. 4, 5 and 6 were also reproduced for the PROBA-V data and provided in the Supplementary data section (Supplementary Figs. 1, 2 and 3).

The NDVI value detected in the spring crop sowing period was higher than expected (i.e. $>$ 0.35), and lower than the reference data in summer, mainly for maize. This was not observed in the results obtained from the synthetic MSR data. These discrepancies come from the input PROBA-V data and not from the SD method itself, as it was also observed in the PROBA-V NDVI time series for the existing pure pixels of the same

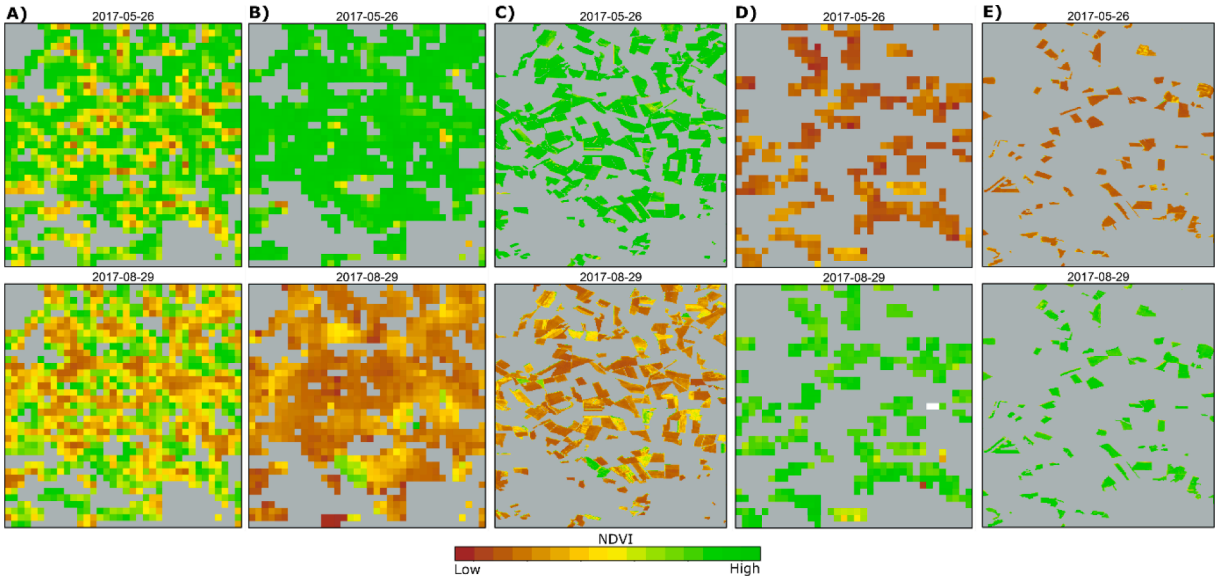

Fig. 4. Disaggregated crop-specific images from synthetic MSR data over a sub-area of interest (shown in Fig. 1). Each column represents: A) Mixel signal, B) Winter cereals disaggregated signal, C) Winter cereals reference signal, D) Maize disaggregated signal and E) Maize reference signal. The top row illustrates a date in late spring (26th May 2017), while the bottom row is for late summer. (29th August 2017). The brown to green color palette represents NDVI values from 0 to 1. Gray color corresponds to non-target mixels. (For interpretation of the references to colour in this figure legend, the reader is referred to the web version of this article.)

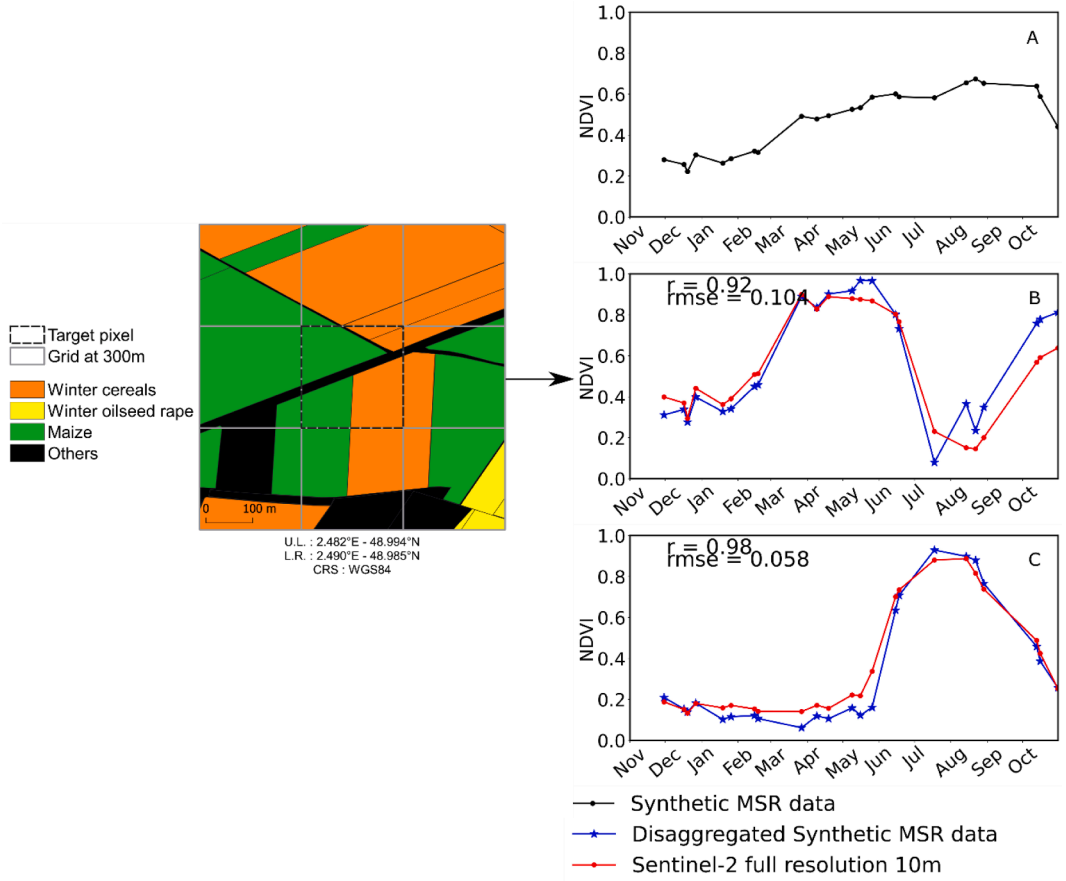

Fig. 5. Comparison between the temporal profile of a disaggregated mixel from synthetic MSR data and the reference profile. The disaggregated mixel is composed of 50% maize, 39% winter cereals and 11% others. A) NDVI temporal profile of the mixel. B) Disaggregated (blue) and reference (red) NDVI temporal profile for Winter cereals. C) Disaggregated (blue) and reference (red) NDVI temporal profile for Maize. (For interpretation of the references to colour in this figure legend, the reader is referred to the web version of this article.)

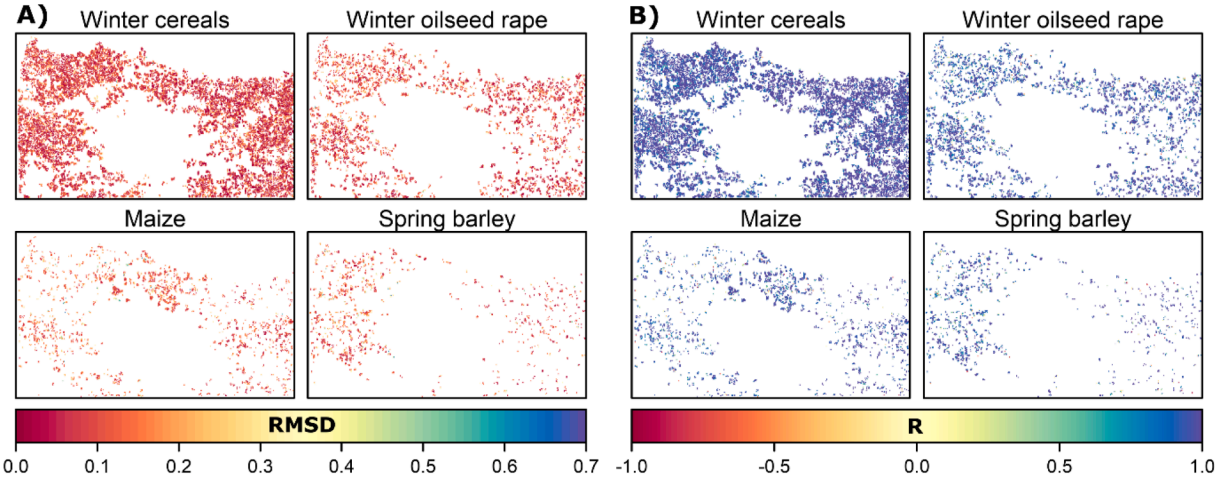

Fig. 6. RMSD (A) and correlation (B) maps between the disaggregated crop-specific NDVI time series from synthetic MSR data and the reference data, for the four main crops (top: Winter cereals, Winter oilseed rape, bottom: Maize, Spring barley).

sensor (Fig. 8). What was revealed here was therefore an inter-sensor divergence that could be due to the Point Spread Function (PSF) of the optical PROBA-V system. Each projected 300 m pixel does not perfectly coincide with the resolution cell, and moreover each resolution cell can be partly affected by its neighbors as the PSF is not a purely rectangle function. In other words, each pixel value can be influenced by its neighbors, that may include other crops but also other permanently vegetated areas (e.g. small tree groups, hedges) that increase the NDVI in winter, or other artificial areas (e.g. buildings, ways) that decrease it in summer. This effect was not considered in this SD method that was based on the image grid geometry.

Altogether the results demonstrated the robustness of the algorithm, even though the relevance of reconstructing the phenological cycle of a given crop was constrained by the quality of the input data. Finally, we

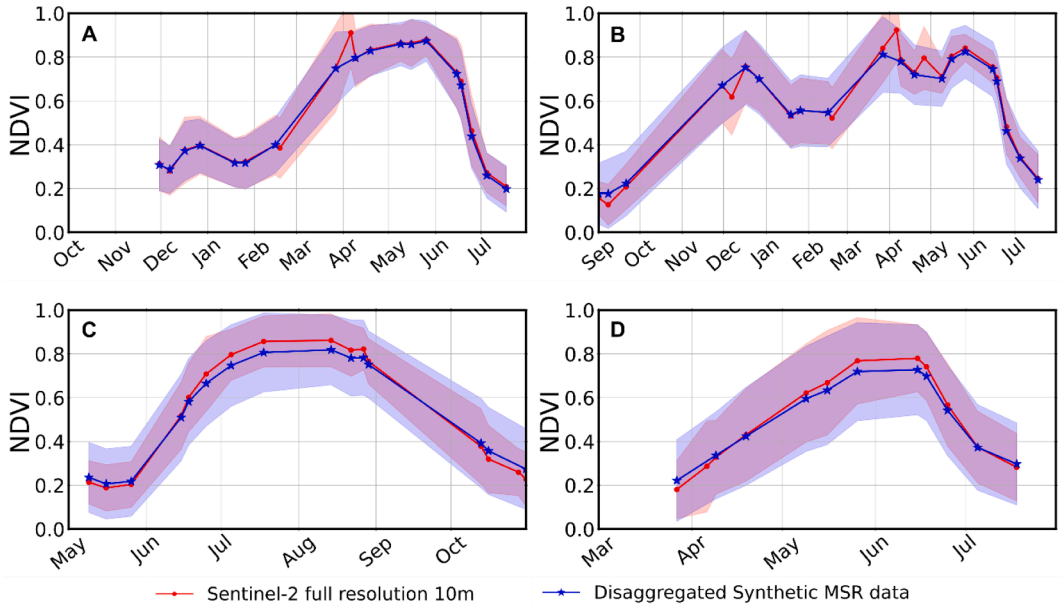

Fig. 7. Average NDVI profiles of all disaggregated mixels from synthetic MSR data (blue) and of all pixels from reference data (red), for the four main crops (A. Winter cereals, B. Winter oilseed rape, C. Maize, D. Spring barley). Shaded band represents the ± 1 standard deviation of values. (For interpretation of the references to colour in this figure legend, the reader is referred to the web version of this article.)

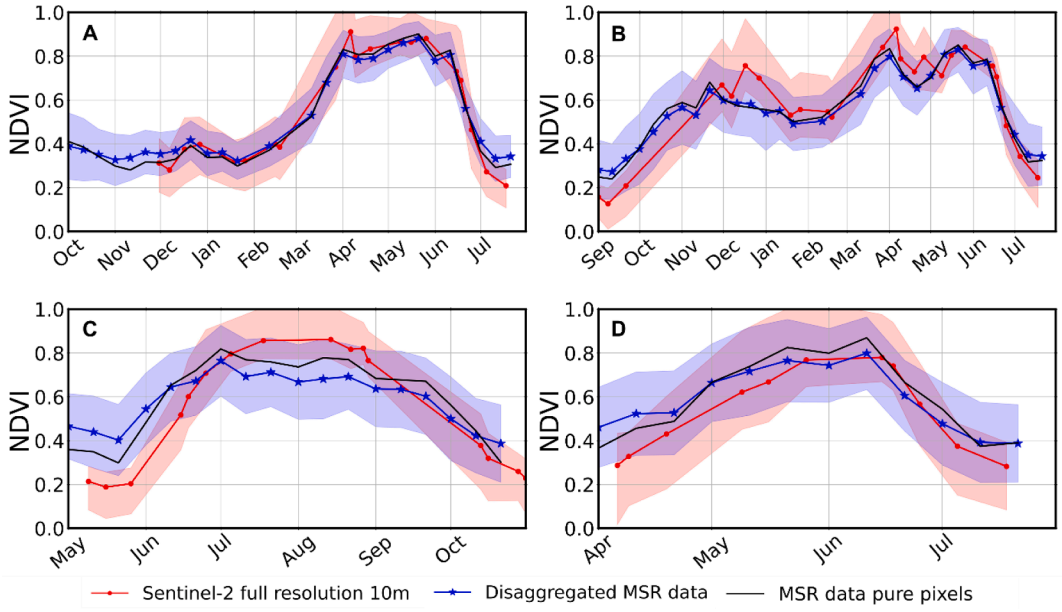

Fig. 8. Average NDVI profile of all disaggregated mixels from PROBA-V data (blue), from pure PROBA-V pixels (black) and reference data (red) for the four main crops (A. Winter cereals, B. Winter oilseed rape, C. Maize, D. Spring barley). The shaded band represents the ± 1 standard deviation of values. (For interpretation of the references to colour in this figure legend, the reader is referred to the web version of this article.)

observed that the method, when it was applied to real MSR data, was able to reconstruct the NDVI curve for the most two dominant crops of the area, winter cereals and winter oilseed rape. It provided a reasonable approximation for maize and spring barley that allowed following the phenological transitions as the SD curve remained correlated with the reference data despite having a smaller seasonal amplitude.

The overall average correlation with the reference data was 0.88 and 0.72 for the synthetic MSR and PROBA-V data respectively. The errors varied from 0.09 to 0.14 for synthetic MSR data and from 0.12 to 0.21 for the PROBA-V data (Table 2).

4. Discussion

SD method allowed estimating the NDVI of all crop types present within a mixel based on knowledge of their fractions. It was possible to obtain the crop-specific NDVI time series at MSR, even if a crop has a small extent within the study area. The results demonstrated that the SD approach was capable of reconstructing the phenological cycle of a given crop. The phenological stages commonly studied by remote sensing data (i.e. SOS, POS and EOS) were clearly visible for all crops.

Table 2
Statistical evaluation of the SD method results summarized for all crops and for each sensor. The values of R, RMSD and Fraction in mixels represent the average value of all analyzed mixels.

	R	RMSD	Number of mixels	Number of pure MSR pixels	Fraction in mixels
Synthetic MSR data					
Winter cereals	0.94	0.09	32 129	254	0.23
Winter oilseed rape	0.89	0.11	11 528	53	0.06
Maize	0.86	0.14	8 087	23	0.03
Spring barley	0.84	0.14	8 084	9	0.03
PROBA-V data					
Winter cereals	0.88	0.12	31 533	267	0.30
Winter oilseed rape	0.81	0.13	11 429	52	0.07
Maize	0.58	0.21	7 818	15	0.04
Spring barley	0.64	0.17	7 903	11	0.04

4.1. Accuracy of crop-specific NDVI

Disaggregated time series showed strong correlations with reference data. The predominant winter crops performed better than the minor spring crops. Spring crops tended to have discrepancies for the extremes values of the reference NDVI curve, especially at the start and middle of their cycle. This may be due to the imprecision of land use information introduced by the "others" class. The intra-class radiometric dissimilarity of the latter could affect the estimate of NDVI of minor crops. The strong presence of winter crops in a neighborhood could explain the fact that these predominant crops were less influenced by this phenomenon. When the SD method is applied to the PROBA-V data, this fact could be worsened by the PSF of its system as observed by Wang and Atkinson (2017) and as mentioned in Section 3.4.

Disaggregated data reproduced the NDVI temporal variations for each crop as confirmed by the reference data. However, the relevance of the observed phenological indicators must be considered with respect to the input data such as the MSR mixel value and the fraction of each crop. In addition, heterogeneous status of a crop within a neighborhood, for the same phenological stage, could affect the NDVI estimation.

4.2. Potential of SD in crop-specific phenology applications

The results demonstrated the robustness of the algorithm and its ability to estimate crop-specific NDVI for all crops. Indeed, the SD approach reinforces the possibility of exploiting the MSR data to study crop phenology over fragmented agricultural areas with a higher number of valid observations and a more regular time step than with high spatial resolution data. This has been demonstrated by PROBA-V data, especially during autumn and spring, when Sentinel-2 images could not be used because of clouds. Moreover, MSR data are available for the last 4 decades, which is fundamental for retrospective studies of the crop-specific phenology, especially in the current context of adaptation of the agricultural production system to climate change. Exploiting MSR data, as proposed by Lobell et al. (2013) and Manfron et al. (2017), can help to improve the understanding of the evolution, or adaptation, of crop growth timing in recent decades.

4.3. Limitations

In this paper, we assumed two key points which were i) full and accurate knowledge of the land use in the mixels and ii) radiometrically homogeneous i-classes. In view of this consideration, firstly it is necessary to reduce the unknown class "others" as much as possible. This will be particularly important for the application of SD at the kilometric spatial resolution of SPOT-VEGETATION which was the predecessor of PROBA-V. Reducing this unknown implies increasing the number of known classes. However, the addition of thematic classes requires the use of a larger sliding window to ensure the amount of mixels needed to solve the system. Increasing the extension of the neighborhood also adds intra-class radiometric differences, because of the spatial variations in phenology for a given crop. Moreover, the addition of classes increases the possibility of having correlations between pixels in the linear equation system, which will impede inversion of the latter. In this context, it is necessary to make a compromise between the number of classes to be processed and the fraction of the class "others" within the mixel. Secondly, the homogeneous condition of the crops is deviated from reality due to many factors (natural or anthropogenic), even for the same phenological stage of a given crop. Indeed, the estimation of NDVI is also sensitive to those factors that may be present in a neighborhood, including the difference in crop density among and within mixels for example. For 1 km spatial resolution images, the notion of intra-class radiometric dissimilarity could be considered as proposed by Busetto et al. (2008). Despite all these above-mentioned limitations, the first sensitivity tests on images at 1 km showed that SD could also reconstruct the phenology of dominant crops, without increasing the number of classes and the size of the neighborhood. The evidence for these observations is not presented in this paper and still has to be validated.

4.4. Perspectives

Vegetation phenology from remote sensing has a wide range of environmental and agricultural applications at local to regional scales, which requires frequent observations with an appropriate spatial resolution. In a fragmented agricultural landscape, SD could provide crop-specific phenology from mixels. In the case of winter wheat, the mapping of phenometrics over a long period could be strongly improved. For example, Manfron et al. (2017) obtained encouraging results for the detection of the date of sowing from MODIS data in a small area in the south of France. For such a study, the SD method could be used as a data pre-processing, at least for the dominant crops.

5. Conclusion

The SD method allowed us to estimate the NDVI of all crop types present in a mixel and to reconstitute the crop-specific phenology from MSR data. The application of the SD on real MSR data demonstrated the robustness of the algorithm.

This is an important result as one of our future research is to apply this method to the study of crop-specific phenology before the Sentinel-2 era, i.e. on SPOT-VEGETATION data. We have established that it will be possible for winter cereals in this current study area, and possibly for other crops in a different region, but only for the most dominant crops. For minor crops, it may be necessary to apply the method to MODIS data because of its 250 m spatial resolution. However, MODIS displays more geometric uncertainty in connection with its whiskbroom design that induces variations in its PSF over the swath direction, which would thus likely increase the effects discussed above, disturbing phenological retrieval from such time series (Helman, 2018).

When applied to PROBA-V data, and presumably also to Sentinel-3 data, the SD method improves the monitoring of individual crops in the context of fragmented landscapes, especially in transition periods such as autumn and spring when cloud cover is often frequent.

CRediT authorship contribution statement

Henry Rivas: Methodology, Software, Validation, Formal analysis, Visualization, Investigation, Writing – original draft. **Nicolas Delbart:**

Supervision, Resources, Writing – review & editing. **Catherine Ottlé:** Conceptualization, Methodology, Resources, Writing – review & editing. **Fabienne Maignan:** Conceptualization, Methodology, Resources, Writing – review & editing. **Emmanuelle Vaudour:** Writing – review & editing, Funding acquisition.

Declaration of Competing Interest

The authors declare that they have no known competing financial interests or personal relationships that could have appeared to influence the work reported in this paper.

Acknowledgments:

Our work was carried out in the framework of the POLYPHEME project through the TOSCA program of the CNES (grant number 200769/id5917). It also strongly benefited from the support of BECAL-Paraguay (grant number 206/2018). The study was initiated when HR and ND were members of the PRODIG research unit which provided initial support.

Appendix A. Supplementary material

Supplementary data to this article can be found online at https://doi.org/10.1016/j.jag.2021.102569.

References

Asner, G.P., Wessman, C.A., Privette, J.L., 1997. Unmixing the directional reflectances of AVHRR sub-pixel landcovers. IEEE Trans. Geosci. Remote Sens. 35, 868–878. https://doi.org/10.1109/36.602529.

Atzberger, C., 2013. Advances in remote sensing of agriculture: context description, existing operational monitoring systems and major information needs. Remote Sens. 5, 949–981. https://doi.org/10.3390/rs5020949.

Atzberger, C., Formaggio, A.R., Shimabukuro, Y.E., Udelhoven, T., Mattiuzzi, M., Sanchez, G.A., Arai, E., 2014. Obtaining crop-specific time profiles of NDVI: the use of unmixing approaches for serving the continuity between SPOT-VGT and PROBA-V time series. Int. J. Remote Sens. 35 (7), 2615–2638. https://doi.org/10.1080/01431161.2014.883106.

Baghdadi, N., Cerdan, O., Zribi, M., Auzet, V., Darboux, F., El Hajj, M., Kheir, R.B., 2008. Operational performance of current synthetic aperture radar sensors in mapping soil surface characteristics in agricultural environments: application to hydrological and erosion modelling. Hydrol. Process. 22 (1), 9–20. https://doi.org/10.1002/(ISSN)1099-108510.1002/hyp.v22:110.1002/hyp.6609.

Becker-Reshef, I., Justice, C., Sullivan, M., Vermote, E., Tucker, C., Anyamba, A., Small, J., Pak, E., Masuoka, E., Schmaltz, J., Hansen, M., Pittman, K., Birkett, C., Williams, D., Reynolds, C., Doorn, B., 2010. Monitoring global croplands with coarse resolution earth observations: the global agriculture monitoring (GLAM) project. Remote Sens. 2, 1589–1609. https://doi.org/10.3390/rs2061589.

Busetto, L., Meroni, M., Colombo, R., 2008. Combining medium and coarse spatial resolution satellite data to improve the estimation of sub-pixel NDVI time series. Remote Sens. Environ. 112 (1), 118–131. https://doi.org/10.1016/j.rse.2007.04.004.

CNES-THEIA LAND, n.d. Muscate – Atelier de distribution. https://theia.cnes.fr (accessed April 26, 2021).

Defourny, P., Bontemps, S., Bellemans, N., Cara, C., Dedieu, G., Guzzonato, E., Hagolle, O., Inglada, J., Nicola, L., Rabaute, T., Savinaud, M., Udroiu, C., Valero, S., Bégué, A., Dejoux, J.-F., El Harti, A., Ezzahar, J., Kussul, N., Labbassi, K., Lebourgeois, V., Miao, Z., Newby, T., Nyamugama, A., Salh, N., Shelestov, A., Simonneaux, V., Traore, P.S., Traore, S.S., Koetz, B., 2019. Near real-time agriculture monitoring at national scale at parcel resolution: Performance assessment of the Sen2-Agri automated system in various cropping systems around the world. Remote Sens. Environ. 221, 551–568. https://doi.org/10.1016/j.rse.2018.11.007.

Delbart, N., Beaubien, E., Kergoat, L., Le Toan, T., 2015. Comparing land surface phenology with leafing and flowering observations from the PlantWatch citizen network. Remote Sens. Environ. 160, 273–280. https://doi.org/10.1016/j.rse.2015.01.012.

Delbart, Nicolas, Kergoat, Laurent, Le Toan, Thuy, Lhermitte, Julien, Picard, Ghislain, 2005. Determination of phenological dates in boreal regions using normalized difference water index. Remote Sens. Environ. 97 (1), 26–38. https://doi.org/10.1016/j.rse.2005.03.011.

Delbart, Nicolas, Le Toan, Thuy, Kergoat, Laurent, Fedotova, Violetta, 2006. Remote sensing of spring phenology in boreal regions: A free of snow-effect method using NOAA-AVHRR and SPOT-VGT data (1982–2004). Remote Sens. Environ. 101 (1), 52–62. https://doi.org/10.1016/j.rse.2005.11.012.

Dodin, M., Smith, H.D., Levavasseur, F., Hadjar, D., Houot, S., Vaudour, E., 2021. Potential of Sentinel-2 Satellite Images for Monitoring Green Waste Compost and Manure Amendments in Temperate Cropland. Remote Sens. 13, 1616. https://doi.org/10.3390/rs13091616.

Donohue, R.J., Lawes, R.A., Mata, G., Gobbett, D., Ouzman, J., 2018. Towards a national, remote-sensing-based model for predicting field-scale crop yield. Field Crops Res. 227, 79–90. https://doi.org/10.1016/j.fcr.2018.08.005.

Faivre, R., Fischer, A., 1997. Predicting Crop Reflectances Using Satellite Data Observing Mixed Pixels. J. Agric. Biol. Environ. Stat. 2, 87–107. https://doi.org/10.2307/1400642.

Foerster, S., Kaden, K., Foerster, M., Itzerott, S., 2012. Crop type mapping using spectral–temporal profiles and phenological information. Comput. Electron. Agric. 89, 30–40. https://doi.org/10.1016/j.compag.2012.07.015.

Gao, F., Anderson, M.C., Zhang, X., Yang, Z., Alfieri, J.G., Kustas, W.P., Mueller, R., Johnson, D.M., Prueger, J.H., 2017. Toward mapping crop progress at field scales through fusion of Landsat and MODIS imagery. Remote Sens. Environ. 188, 9–25. https://doi.org/10.1016/j.rse.2016.11.004.

Gao, F., Masek, J., Schwaller, M., Hall, F., 2006. On the blending of the Landsat and MODIS surface reflectance: predicting daily Landsat surface reflectance. IEEE Trans. Geosci. Remote Sens. 44, 2207–2218. https://doi.org/10.1109/TGRS.2006.872081.

Gevaert, C.M., García-Haro, F.J., 2015. A comparison of STARFM and an unmixing-based algorithm for Landsat and MODIS data fusion. Remote Sens. Environ. 156, 34–44. https://doi.org/10.1016/j.rse.2014.09.012.

Haertel, V.F., Shimabukuro, Y.E., 2005. Spectral linear mixing model in low spatial resolution image data. IEEE Trans. Geosci. Remote Sens. 43 (11), 2555–2562. https://doi.org/10.1109/TGRS.2005.848692.

Helman, D., 2018. Land surface phenology: What do we really 'see' from space? Sci. Total Environ. 618, 665–673. https://doi.org/10.1016/j.scitotenv.2017.07.237.

Heupel, Katharina, Spengler, Daniel, Itzerott, Sibylle, 2018. A Progressive Crop-Type Classification Using Multitemporal Remote Sensing Data and Phenological Information. PFG –. J. Photogramm. Remote Sens. Geoinformation Sci. 86 (2), 53–69. https://doi.org/10.1007/s41064-018-0050-7.

Holben, B.N., 1986. Characteristics of maximum-value composite images from temporal AVHRR data. Int. J. Remote Sens. 7 (11), 1417–1434. https://doi.org/10.1080/01431168608948945.

Kastens, J.H., Brown, J.C., Coutinho, A.C., Bishop, C.R., Esquerdo, J.C.D.M., 2017. Soy moratorium impacts on soybean and deforestation dynamics in Mato Grosso, Brazil. PLOS ONE 12, e0176168. 10.1371/journal.pone.0176168.

Khaliq, A., Peroni, L., Chiaberge, M., 2018. Land cover and crop classification using multitemporal sentinel-2 images based on crops' phenological cycle, in: 2018 IEEE Workshop on Environmental, Energy, and Structural Monitoring Systems (EESMS). In: Presented at the 2018 IEEE Workshop on Environmental, Energy, and Structural Monitoring Systems (EESMS), pp. 1–5. https://doi.org/10.1109/EESMS.2018.8405830.

Leenhardt, D., Therond, O., Mignolet, C., 2012. Quelle représentation des systèmes de culture pour la gestion de l'eau sur un grand territoire ? Agron. Environ. Sociétés 2, 77–89 (in French).

Li, W., Baret, F., Weiss, M., Buis, S., Lacaze, R., Demarez, V., Dejoux, J., Battude, M., Camacho, F., 2017. Combining hectometric and decametric satellite observations to provide near real time decametric FAPAR product. Remote Sens. Environ. 200, 250–262. https://doi.org/10.1016/j.rse.2017.08.018.

Lobell, D.B., 2013. The use of satellite data for crop yield gap analysis. Field Crops Res., Crop Yield Gap Anal. – Rationale Methods Appl. 143, 56–64. https://doi.org/10.1016/j.fcr.2012.08.008.

Lobell, D.B., Ortiz-Monasterio, J.I., Sibley, A.M., Sohu, V.S., 2013. Satellite detection of earlier wheat sowing in India and implications for yield trends. Agric. Syst. 115, 137–143. https://doi.org/10.1016/j.agsy.2012.09.003.

Lobell, D.B., Thau, D., Seifert, C., Engle, E., Little, B., 2015. A scalable satellite-based crop yield mapper. Remote Sens. Environ. 164, 324–333. https://doi.org/10.1016/j.rse.2015.04.021.

Lobell, David B., Asner, Gregory P., 2004. Cropland distributions from temporal unmixing of MODIS data. Remote Sens. Environ. 93 (3), 412–422. https://doi.org/10.1016/j.rse.2004.08.002.

Manfron, G., Delmotte, S., Busetto, L., Hossard, L., Ranghetti, L., Brivio, P.A., Boschetti, M., 2017. Estimating inter-annual variability in winter wheat sowing dates from satellite time series in Camargue, France. Int. J. Appl. Earth Obs. Geoinformation 57, 190–201. https://doi.org/10.1016/j.jag.2017.01.001.

Mulla, David J., 2013. Twenty five years of remote sensing in precision agriculture: Key advances and remaining knowledge gaps. Biosyst. Eng Special Issue: Sens. Technol. Sustain. Agric. 114 (4), 358–371. https://doi.org/10.1016/j.biosystemseng.2012.08.009.

Oleson, K.W., Sarlin, S., Garrison, J., Smith, S., Privette, J.L., Emery, W.J., 1995. Unmixing multiple land-cover type reflectances from coarse spatial resolution satellite data. Remote Sens. Environ. 54 (2), 98–112. https://doi.org/10.1016/0034-4257(95)00100-F.

Petrou, Zisis I., Manakos, Ioannis, Stathaki, Tania, 2015. Remote sensing for biodiversity monitoring: a review of methods for biodiversity indicator extraction and assessment of progress towards international targets. Biodivers. Conserv. 24 (10), 2333–2363. https://doi.org/10.1007/s10531-015-0947-z.

Sakamoto, Toshihiro, Van Nguyen, Nhan, Ohno, Hiroyuki, Ishitsuka, Naoki, Yokozawa, Masayuki, 2006. Spatio–temporal distribution of rice phenology and cropping systems in the Mekong Delta with special reference to the seasonal water flow of the Mekong and Bassac rivers. Remote Sens. Environ. 100 (1), 1–16. https://doi.org/10.1016/j.rse.2005.09.007.

Sakamoto, T., Yokozawa, M., Toritani, H., Shibayama, M., Ishitsuka, N., Ohno, H., 2005. A crop phenology detection method using time-series MODIS data. Remote Sens. Environ. 96 (3-4), 366–374. https://doi.org/10.1016/j.rse.2005.03.008.

Settle, J.J., Drake, N.A., 1993. Linear mixing and the estimation of ground cover proportions. Int. J. Remote Sens. 14, 1159–1177. 10.1080/01431169308904402.

Siachalou, S., Mallinis, G., Tsakiri-Strati, M., 2015. A Hidden Markov Models Approach for Crop Classification: Linking Crop Phenology to Time Series of Multi-Sensor Remote Sensing Data. Remote Sens. 7, 3633–3650. https://doi.org/10.3390/rs70403633.

Solano-Correa, Y.T., Bovolo, F., Bruzzone, L., Fernández-Prieto, D., 2018. Automatic Derivation of Cropland Phenological Parameters by Adaptive Non-Parametric Regression of Sentinel-2 Ndvi Time Series. In: IGARSS 2018–2018 IEEE International Geoscience and Remote Sensing Symposium. Presented at the IGARSS 2018–2018 IEEE International Geoscience and Remote Sensing Symposium, pp. 1946–1949. https://doi.org/10.1109/IGARSS.2018.8519264.

IGN, 2021. Géoservices. https://geoservices.ign.fr (accessed April 26, 2021).

Vaudour, Emmanuelle, Gomez, Cécile, Lagacherie, Philippe, Loiseau, Thomas, Baghdadi, Nicolas, Urbina-Salazar, Diego, Loubet, Benjamin, Arrouays, Dominique, 2021. Temporal mosaicking approaches of Sentinel-2 images for extending topsoil organic carbon content mapping in croplands. Int. J. Appl. Earth Obs. Geoinformation 96, 102277. https://doi.org/10.1016/j.jag.2020.102277.

Vaudour, E., Noirot-Cosson, P.E., Membrive, O., 2015. Early-season mapping of crops and cultural operations using very high spatial resolution Pléiades images. Int. J. Appl. Earth Obs. Geoinformation 42, 128–141. https://doi.org/10.1016/j.jag.2015.06.003.

VITO, 2018. VITO Earth Observation – Product Distribution Portal. https://www.vito-eodata.be (accessed April 26, 2021).

Waldner, F., Fritz, S., Di Gregorio, A., Plotnikov, D., Bartalev, S., Kussul, N., Gong, P., Thenkabail, P., Hazeu, G., Klein, I., Löw, F., Miettinen, J., Dadhwal, V.K., Lamarche, C., Bontemps, S., Defourny, P., 2016. A Unified Cropland Layer at 250 m for Global Agriculture Monitoring. Data 1, 3. https://doi.org/10.3390/data1010003.

Wang, Q., Atkinson, P.M., 2017. The effect of the point spread function on sub-pixel mapping. Remote Sens. Environ. 193, 127–137. https://doi.org/10.1016/j.rse.2017.03.002.

Ward, M H, Nuckols, J R, Weigel, S J, Maxwell, S K, Cantor, K P, Miller, R S, 2000. Identifying populations potentially exposed to agricultural pesticides using remote sensing and a Geographic Information System. Environ. Health Perspect. 108 (1), 5–12. https://doi.org/10.1289/ehp.001085.

Weiss, M., Jacob, F., Duveiller, G., 2020. Remote sensing for agricultural applications: A meta-review. Remote Sens. Environ. 236, 111402. https://doi.org/10.1016/j.rse.2019.111402.

Wu, Bingfang, Meng, Jihua, Li, Qiangzi, Yan, Nana, Du, Xin, Zhang, Miao, 2014. Remote sensing-based global crop monitoring: experiences with China's CropWatch system. Int. J. Digit. Earth 7 (2), 113–137. https://doi.org/10.1080/17538947.2013.821185.

Zhao, Y., Huang, B., Song, H., 2018. A robust adaptive spatial and temporal image fusion model for complex land surface changes. Remote Sens. Environ. 208, 42–62. https://doi.org/10.1016/j.rse.2018.02.009.

Zhukov, B., Oertel, D., Lanzl, F., Reinhackel, G., 1999. Unmixing-based multisensor multiresolution image fusion. IEEE Trans. Geosci. Remote Sens. 37, 1212–1226. https://doi.org/10.1109/36.763276.